NANO LETTERS

Cite This: Nano Lett. 2019, 19, 4827−4835

Mini Review

pubs.acs.org/NanoLett

Interferometric Scattering Microscopy: Seeing Single Nanoparticles and Molecules via Rayleigh Scattering

Richard W. Taylor and Vahid Sandoghdar*

Max Planck Institute for the Science of Light and Max-Planck-Zentrum für Physik und Medizin, 91058 Erlangen, Germany

ABSTRACT: Fluorescence microscopy has been the workhorse for investigating optical phenomena at the nanometer scale but this approach confronts several fundamental limits. As a result, there have been a growing number of activities toward the development of fluorescent-free imaging methods. In this Mini Review, we demonstrate that elastic scattering, the most ubiquitous and oldest optical contrast mechanism, offers excellent opportunities for sensitive detection and imaging of nanoparticles and molecules at very high spatiotemporal resolution. We present interferometric scattering (iSCAT) microscopy as the method of choice, explain its theoretical foundation, discuss its experimental nuances, elaborate on its deep connection to bright-field imaging and other established microscopies, and discuss its promise as well as challenges. A showcase of numerous applications and avenues made possible by iSCAT demonstrates its rapidly growing impact on various disciplines concerned with nanoscopic phenomena.

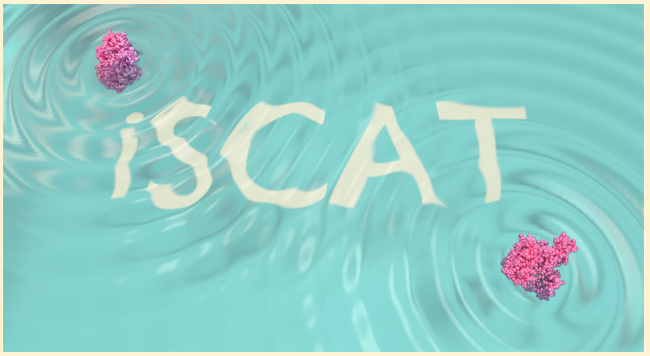

KEYWORDS: *Rayleigh scattering, interferometric microscopy, iSCAT, extinction, protein sensing*

Pioneering room-temperature studies of single molecules, quantum dots, and color centers have all been based on the detection of fluorescence. Fluorescence provides the crucial benefit that molecules can be detected on a low background with a certain degree of specificity through their characteristic spectra. However, fluorescence microscopy is accompanied by several restrictions including (1) limited photoemission caused by photobleaching, which prevents long measurements, (2) finite fluorescence rate (saturation), which limits speed, (3) photoblinking, which might hinder continuous observations, as well as (4) the need for labeling, which may introduce artifacts to the interpretation. As a result, many efforts have been launched for fluorescence-free detection of matter down to the single-molecule level. In this Mini Review, we discuss the developments of the past two decades, which have led to the label-free detection of nanoparticles including single dye molecules, semiconductor quantum dots, viruses, and small proteins through interferometric scattering (iSCAT) microscopy. A thorough account can be found in ref 1.

Extinction Measurements down to Single-Molecule Sensitivity. Extinction of a beam, be it of light, sound or material particles, is usually formulated in the context of the Optical Theorem (OT).[2] Often rendered as extinction = absorption + scattering, the OT states that the energy taken out of a plane wave with a well-defined wavevector $\mathbf{k}$ is either due to absorption, that is, transfer of energy to other channels, or due to scattering into other $\mathbf{k}$-vectors. When attempting to detect a small object in extinction, it is desirable to focus the incident beam tightly to reach the most favorable ratio of the object cross-section to the beam area, σ/A (see Figure 1a). In this situation, the application of the OT becomes nontrivial since a large number of $\mathbf{k}$ vectors and strong polarization gradients are involved in the tight focus. Nevertheless, rigorous calculations show that even one atom can fully extinguish a focused laser beam,[3] thus testifying to the fundamentally efficient nature of Rayleigh scattering as a light-matter interaction mechanism.

A more informative picture of the extinction process is based on the realization that the signal on the detector consists of an intensity, which stems from the sum of the fields associated with the incident beam (E_i) and those scattered by the object (E_s)

$$P_d \propto |E_i + E_s|^2 = |E_i|^2 + |E_s|^2 + 2\mathcal{R}(E_i E_s^*) \quad (1)$$

where P_d denotes the power detected. Thus, for a high degree of extinction to occur, the cross-term has to annul the first two positive terms, leading to destructive interference in the forward direction. In this picture, it becomes clear that spatial mode matching between the wavefronts of E_i and E_s is a critical requirement for perfect extinction. In the case of a subwavelength object, the incident wavefronts should match a dipolar emission pattern.[2,3] Indeed, decomposing a focused laser beam into multipoles shows that the tighter the focus, the higher the contribution of the dipole component.[4] In other

Received: May 3, 2019
Revised: July 6, 2019
Published: July 17, 2019

DOI: 10.1021/acs.nanolett.9b01822
Nano Lett. 2019, 19, 4827−4835

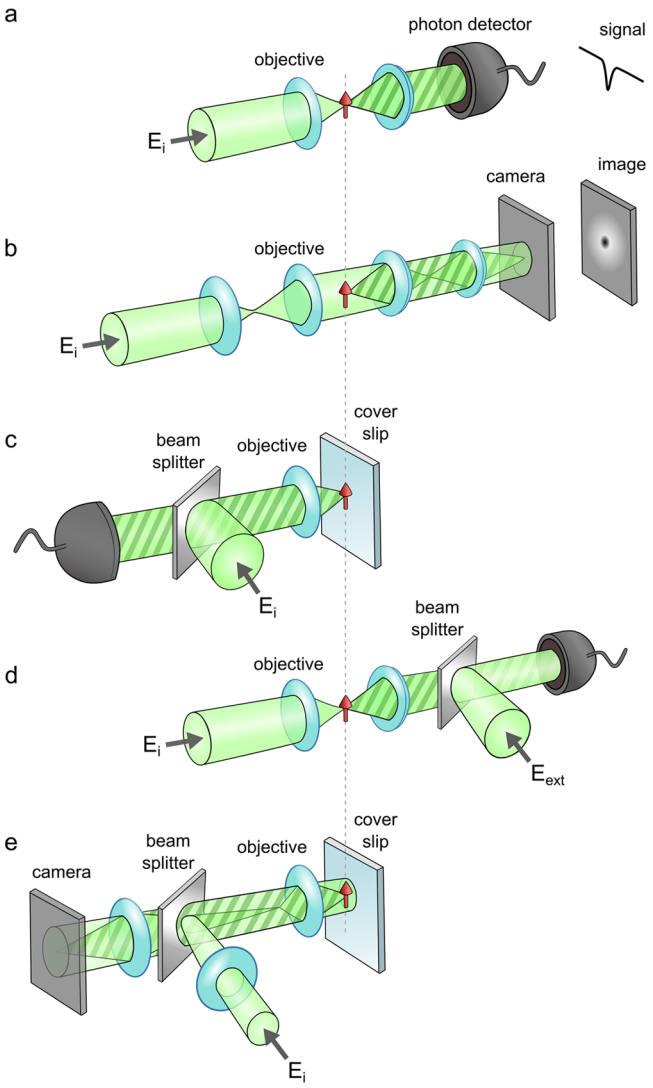

Figure 1. Various schemes for illumination and detection. Red arrow represents the dipole moment associated with a nano-object. Light green and shaded areas indicate the illumination (E_i) and the scattered fields (E_s), respectively. (a) Point detection in transmission via focused illumination. A typical extinction dip using such a detection scheme is sketched. (b) Wide-field illumination and transmission detection on an imaging camera. Again, a typical extinction image is depicted. (c) A reflection-based scheme for point detection with illumination similar to (a). (d) Point detection in transmission with focused illumination, similar to (a) but with an external reference beam of field (E_{ext}). (e) A scheme of illumination and wide-field imaging by means of reflection, equivalent to a folded version of (b).

words, optimization of the metric σ/A and spatial mode matching are two sides of the same coin.

The general case of subwavelength nanoparticles can be treated by considering the scattering and absorption cross sections, given by $\sigma_{sca} = \frac{8}{3}\pi^2|\alpha|^2(\lambda_m)^{-4}$ and $\sigma_{abs} = \frac{2\pi}{\lambda_m}\mathrm{Im}(\alpha)$, respectively, where

$$\alpha = 3\epsilon_m V\left(\frac{\epsilon_p - \epsilon_m}{\epsilon_p + 2\epsilon_m}\right) \quad (2)$$

denotes the complex particle polarizability.[2] Here, V denotes particle volume, λ_m signifies the wavelength in the medium whereas ϵ_p and ϵ_m are the permittivities of the particle and the embedding medium, respectively. The wavelength-dependent complex quantities ϵ_p and ϵ_m determine the balance between absorption and scattering contributions. We note that the key quantity that generates the signal on the detector is $E_s = \alpha E_i$. Therefore, because the real and imaginary parts of ϵ_p are connected through the Kramer−Kronig relations, absorption is also encoded in the amplitude and phase of E_s.[2] We also remark that although plasmon resonances in materials such as silver and gold enhance scattering, the magnitude of α is predominantly determined by the particle volume V. Here, it should be noted that the highest plasmonic effects in the visible range lead to about a 10-fold increase in the scattering cross-section for silver, corresponding to about a factor of 3 in α. This plasmonic advantage can be compensated by a mere increase of 45% in the particle radius.

In the ideal case of a two-level emitter illuminated by monochromatic light resonant with its transition at wavelength λ, elementary treatments show that the extinction cross-section amounts to $\sigma_0 = 3\lambda^2/2\pi$.[5] Considering that light can be focused to about $A \approx (\lambda/2)^2$, given by the diffraction limit, a single molecule would be expected to cast a significant shadow on the laser beam. Indeed, recent cryogenic experiments have reported on extinction dips of about 10% from single dye molecules.[6] In the case of single emitters at room temperature, σ_0 is reduced by a factor in the order of 10^{-5} due to thermal agitations which lead to dephasing of the dipole moment. Nevertheless, as we will show in later sections, single semiconductor quantum dots and dye molecules can be detected in direct extinction.[7,8]

In fact, it turns out that even the conventional bright-field configuration is suitable for detecting extinction with very high sensitivity. Here, as depicted in Figure 1b, a laser beam is focused in the back focal plane of a microscope objective to generate plane-wave illumination on the sample. A second objective collimates the scattering from a nano-object into a tube lens which images it onto a camera screen. The laser beam is rendered back to a plane wave, illuminating a large area on the camera. The wavefronts are maximally mismatched so that only a small fraction of the incident power interferes with the scattered light within the microscope point-spread function (PSF). Although the interaction is not very efficient, even a very weak image spot corresponding to a single protein can be detected because the illumination is spread over a large area, leading to a correspondingly weak background.

Nevertheless, standard bright-field arrangements are not used for sensitive extinction imaging because the eye, and even most modern detectors simply do not have the required dynamic range to process a small signal on a large background.[1] This led many scientists to invent clever strategies such as dark-field, phase contrast, and differential interference contrast (DIC) microscopies.[1] Interestingly, however, these methods did not push the limits of detection sensitivity with regard to the achievable signal-to-noise ratio (SNR). Instead, they merely provided convenient ways of identifying image features within the limitations of the available detectors.

At the turn of the twenty-first century, single-molecule detection relied on fluorescence, and detection of non-fluorescent nanoparticles, for example, gold or silver, was achieved solely via dark-field microscopy. Here, it is important to realize that the decisive parameter for fluorescence detection of single molecules is a high quantum efficiency, defined as

DOI: 10.1021/acs.nanolett.9b01822
Nano Lett. 2019, 19, 4827−4835

$\frac{\gamma_r}{\gamma_r+\gamma_{nr}}$, where γ_r and γ_{nr} represent the radiative and nonradiative decay rates, respectively. For extinction measurements, however, the metric of interest is the extinction cross-section given by $\sigma = \frac{3\lambda^2}{2\pi} \times \frac{\gamma_r}{\gamma_r+\gamma_{nr}+\gamma_{deph}}$. At room temperature, the latter quotient amounts to about 10^{-6} to 10^{-5} for nearly all common cases of emitters embedded in a solid, where the dephasing rate γ_{deph} is the dominating factor. Thus, it follows that even if $\gamma_{nr} \approx 1000\gamma_r$ (i.e., very strong quenching), the extinction cross-section does not change substantially whereas such conditions would render fluorescence detection impossible. Thus, extinction opens a large number of doors for exploring nonfluorescent matter.

In 2001, Plakhotnik and Palm reported on an interesting cryogenic experiment wherein signatures of single dye molecules were detected via interference between their scattering and a residual reflection of the excitation laser beam.[9] In 2002, Orrit, Lounis, and colleagues showed a room-temperature method that took advantage of light absorption for detecting small gold nanoparticles (GNPs) based on the photothermal effect.[10] Here, a laser beam was used to heat a nanoparticle, which in turn changed the temperature and, thus, the index of refraction of its environment. A second laser beam was then used to detect the index change via heterodyne interferometry. In 2004, Sandoghdar et al., introduced iSCAT microscopy.[11] Using a common-path interferometer in a simple reflection arrangement (see Figure 1c), a supercontinuum laser beam was used to image GNPs down to a diameter of 5 nm and record their plasmon spectra. Later that year, Arbouet and co-workers reported on a lock-in assisted measurement of the transmitted light (see Figure 1a) for detecting GNPs down to 10 nm.[12] In 2006, Ignatovich and Novotny showed the detection of single viruses in a microfluidic channel via interference with an external laser beam[13] (see Figure 1d). In the same year, wide-field (see Figure 1e) and microsecond imaging capability of iSCAT were also demonstrated.[14] A more complete account of these and related developments is found in ref 1.

The physical principles and techniques that are employed in the above-mentioned efforts were already well understood a century earlier in terms of reflection, absorption, and transmission from bulk measurements. However, researchers had to improve their experimental techniques and adapt their theoretical understanding to the concept of "scattering" to become sensitive to individual nonfluorescent molecules. Indeed, the general wisdom prior to the above-mentioned developments in the 2000s was that single molecules and small nanoparticles could not be detected via extinction.

Interferometric Scattering (iSCAT) Detection. The principal concept in interferometric microscopy is the superposition of a reference light field $\mathbf{E}_r = E_r e^{i\phi_r}$ with the field emerging from the sample. Let us consider a field $\mathbf{E}_s = E_s e^{i\phi_s}$ scattered from a subwavelength object. The detected power reads

$$P_d \propto I_d = |E_r + E_s|^2 = I_r + I_s + 2E_rE_s \cos\phi \tag{3}$$

The first of the three resulting components denotes the contribution of the reference field ($I_r = |E_r|^2$), whereas the second and third terms represent the contributions of the pure scattering power from the object ($I_s = |E_s|^2$) and the cross-term ($2E_rE_s \cos\phi$) with $\phi = \phi_r - \phi_s$. This phase contains a sinusoidal component that describes the propagation phase, a Gouy phase caused by the variations of wavevectors, and a phase contribution determined by the dielectric function of the nano-object.[11]

Considering the proportionality of E_s to α, one notes that I_s drops with the sixth power of the particle size. The signal from a 5 nm particle is, therefore, one million times smaller than that of a particle with a diameter of 50 nm. Because the cross-term in eq 3 is linearly proportional to E_s, it dominates I_s for small E_s. Thus, to access the information about the particle, one can consider the detected signal with and without the particle of interest to arrive at the contrast

$$c = \frac{I_d - I_r}{I_r} = \frac{2E_sE_r \cos\phi}{I_r} = 2\frac{E_s}{E_r}\cos\phi \tag{4}$$

We emphasize that E_r represents any kind of reference field, for example, the incident field in conventional extinction (see Figure 1a) or an external reference (see Figure 1d), including both homodyne (at the same frequency) and heterodyne (with a frequency offset) detection schemes. We also point out that an iSCAT measurement performed in reflection (see Figure 1c) can be considered as a folded version of an extinction experiment (see Figure 1a). In this sense, we consider iSCAT as an umbrella nomenclature for any interferometric mechanism used to detect small nanoparticles via scattering.

The expression in eq 4 might lead one to imply that a better sensitivity could be achieved if one minimized E_r in the denominator. In fact, one can adopt an optical arrangement, where E_r is adjustable at will, for example, by employing a separate reference arm (see Figure 1d). However, the increase in contrast that results is accompanied by a smaller overall signal, which leads to a lower SNR in the shot-noise limit.[11] Moreover, a scheme using a separate arm is more susceptible to mechanical instabilities. Nevertheless, engineering of the balance between E_r and E_s can be advantageous for practical reasons.[15,16]

Long and Fast Measurements. One of the main shortcomings of fluorescence microscopy is a limited observation time imposed by photobleaching. However, the scattering signal does not degrade over time because the illumination wavelength is typically far from any absorption resonances in the sample, regardless of whether one uses the inherent scattering of a bioparticle or detects a GNP. Thus, very long measurement times become feasible.

Another decisive advantage of scattering over fluorescence is the lack of saturation. The lifetime of the excited state in a fluorophore imposes a bottleneck on the rate at which it can radiate, thus limiting how fast one can image. Scattering, however, does not suffer from such saturation because it is a linear process so that a stronger illumination yields higher scattering rates. Indeed, up to 1 MHz imaging speed has been demonstrated in iSCAT, limited only by the availability of suitable cameras.[14,17,18] Furthermore, one should keep in mind that the finite absorption cross-section of biological matter puts a limit on acceptable illumination intensities on live cells, depending on many parameters such as the cell type and phase in its life cycle, the illumination wavelength, modality (continuous-wave or pulsed), and duration.[19] To give a flavor of the illumination power used in iSCAT, we point out that the fastest imaging in ref 20 required less than 10 kW/cm^2 at a wavelength of 550 nm.

Background Removal. In fluorescence microscopy highly efficient spectral filtering eliminates spurious background light.

DOI: 10.1021/acs.nanolett.9b01822
Nano Lett. 2019, 19, 4827−4835

Similarly, spatial filtering, rather than spectral filtering, is also a necessity for dark-field microscopy. The background in iSCAT constitutes an integral part of the signal (see eq 3) facing the particular challenge that slight lateral changes in the topography or refractive index of the sample or substrate introduce a speckle-like pattern (see Figure 2a). This background needs to be subtracted to arrive at the desired information about the nanoparticle under study. Some of the technical difficulties in doing so involve eliminating the temporal fluctuations in the illumination and addressing the limited dynamic range of the detector.[1]

In dynamic studies, the background can be conveniently eliminated if the particle of interest appears on the sample or moves within it faster than the changes in the background. Here, consecutive images can be differentially subtracted to remove the stationary part of the image,[21,22] as illustrated in Figure 2a. In practice, different variations of this method can be used. For example, a temporal median intensity can be subtracted,[23] an iterative-estimation algorithm is used,[24] or one averages rolling windows across stacks of frames.[25] For situations where the background possesses spatiotemporal dynamics as is the case for live biological specimens, more sophisticated image processing must be used.[20]

We note that one could equally well apply these background treatment methods to dark-field microscopy. In fact, the shot-noise-limited SNR in interferometric detection is only a factor of 2 better than that in dark-field detection. In practice, however, ultrasensitive dark-field detection is challenging because the sixth-power dependence of the signal on the particle size places higher demands on the dynamic range and sensitivity of detectors than with iSCAT.

Detection Sensitivity. Any sensitive measurement is ultimately limited by random signal fluctuations, which we call "noise". The most prominent noise sources are the instrumental laser power fluctuation and beam pointing instability. To detect iSCAT contrasts smaller than about 10^{-3}, laser intensity fluctuations would have to be accounted for via referencing or normalization. In the case of confocal imaging with use of a point detector, one can use a balanced photodiode pair to reach a stability in the order of 10^{-7}.[8,26] In camera-based imaging, the total power recorded within each frame can serve to similarly account for intraframe fluctuations. However, beyond the instrumental noise sources, photon number fluctuations in a laser beam given by the so-called shot noise ($\sqrt{N}$ for an average of N photons) put a fundamental limit on any measurement.[5]

It is worth mentioning that iSCAT measurements can be extremely robust against mechanical instabilities if the reference and the scattering beams share common paths. Nevertheless, lateral vibrations might compromise ultrasensitive measurements because even a few nanometers of motion suffice to change the differential contrast that results from imperfect background subtraction.[27]

Nanometer Lateral and Axial Localization Precision. As in fluorescence microscopy, the center of an iSCAT-PSF can be determined within the available SNR to localize the lateral position of a nanoparticle. As we will see below, this has been exploited to track viruses and gold nanoparticles with nanometer precision at unprecedented speeds. However, the major asset of iSCAT imaging is in its sensitivity to the phase ϕ in eq 3, giving access to information on nanometer axial displacements. To this end, reflection mode iSCAT offers the best axial iSCAT resolution (see Figure 1c,e), where the scatterer can accumulate a traveling phase. The first realizations of this nanoholographic feature were reported in

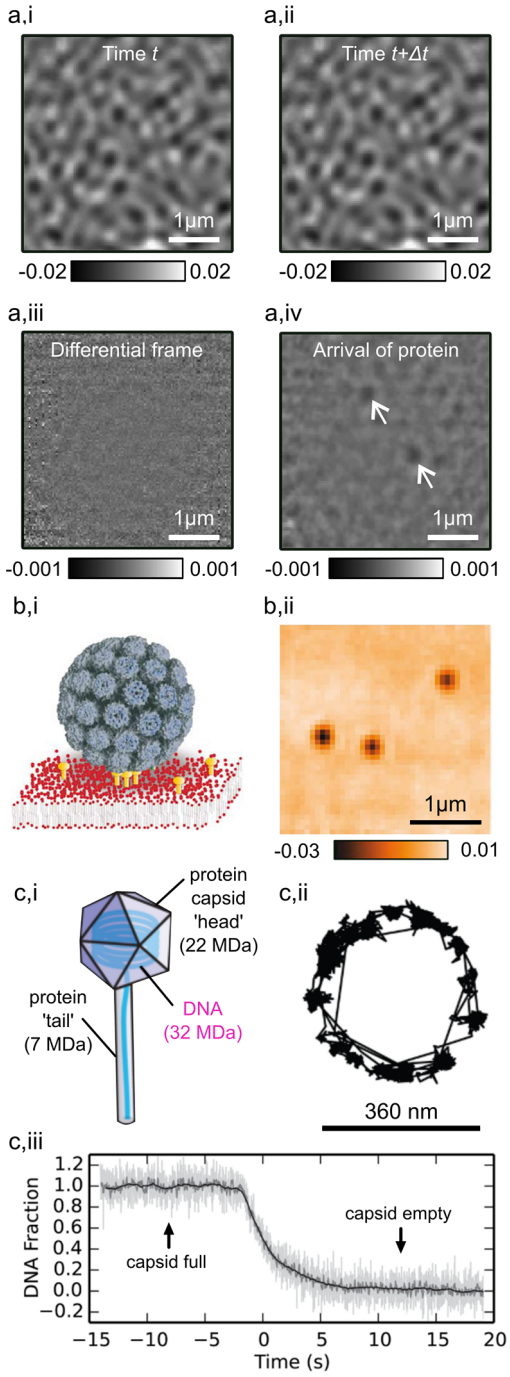

Figure 2. iSCAT image of a bare coverslip recorded at a time t (a,i) and of the same area recorded at a later time $t + \Delta t$ (a,ii). Subtraction of the image acquired at time $t + \Delta t$ from the earlier frame removes static background features (a,iii). Dynamic arrival of two proteins registers in the differential frame (a,iv, marked with arrows). Adapted from ref 21. Illustration of a SV40 virus bound to ganglioside (GM1)-tagged lipids in an artificial lipid bilayer (b,i). An iSCAT image of single SV40 virions attached to a lipid bilayer on a coverslip (b,ii), adapted from ref 22. Illustration of a bacteriophage showing head and tail geometry (c,i). A trajectory from the head of a single bacteriophage whereas its tail is adsorbed to the surface (c,ii). Following stimulation, the DNA content of the capsid head is ejected over time (c,iii), as determined through the diminishing iSCAT contrast. Adapted from ref 44.

DOI: 10.1021/acs.nanolett.9b01822
Nano Lett. 2019, 19, 4827−4835

refs 28 and 29. However, the ambiguity associated with the periodic nature of ϕ limited the detectable displacements to values below 100 nm. More recently, it has been shown that the evolution of the PSF rings and their contrasts can provide crucial information about the particle's axial position over several micrometers.[20] A particularly fruitful situation arises in the case of wide-field illumination where planar and spherical waves interfere to produce rings around the main PSF spot on the camera.[20,30]

Illumination and Detection Arrangements. In the first iSCAT studies, the laser focus was scanned across the sample and the iSCAT signal was recorded on a point detector.[11] However, this was soon extended to wide-field[14] and fast beam-scanning[22] illumination schemes combined with camera detection. These modes can be operated with the detector either placed in transmission or in reflection to match the needs of each study (see Figure 1).

For example, an important advantage of reflection iSCAT is its exquisit sensitivity to the axial position of the nanoparticle. In transmission measurements, on the other hand the background speckle is reduced because E_r and E_s experience smaller phase difference.[1] This feature was combined with index matching to detect single small organic molecules[8,26] and for imaging in cells.[31]

Another important point to realize is that iSCAT measurements do not necessarily require laser illumination. Any light source can be used as long as the coherence length of the light is sufficiently large compared to the separation between the scatterer and the location where the reference is picked up. Indeed, nanoparticles very close to a cover glass can also be detected with iSCAT using incoherent sources such as LEDs.[32]

Applications requiring fast imaging are best suited for wide-field illumination and camera-based detection, which can reach speeds of several tens of kilohertz up to megahertz. This is far faster than scanning schemes, be they based on piezoelectric actuators[11,26,33] or acousto-optical deflectors.[7,17,18,34] The iSCAT contrast can be enhanced in the reflection mode because the reference field becomes weaker. To improve the contrast for real-time inspection, spatial masks have recently been introduced.[15,16]

Applications. *Gold Nanoparticles.* Gold nanoparticles (GNPs) have played an important role in the development of iSCAT because they are interesting for plasmonic applications and can be used as inert and stable biological labels. The early experiments detected GNPs as small as 5 nm[11,14] limited by the speckle background that is generated by the underlying glass substrate. Recently, GNPs as small as 2 nm in diameter were imaged with iSCAT.[35]

Some of the iSCAT studies performed on GNPs include the retrieval of the complex dielectric function of a single particle as small as 10 nm over the visible spectrum,[36] determining the orientation of ellipsoidal nanorods through polarized detection,[37] and mapping occupation probability within microfludic slit channels.[29,38] Further examples of two and three-dimensional tracking of GNPs will be discussed below.[17,18,20,23,39−42]

Semiconductor Colloids. Semiconductor nanocrystal quantum dots act as artificial atoms and have applications in many areas of science and technology, including bioimaging. These nanoparticles with typical diameters of a few nanometers and extinction cross sections in the order of 10^{-15} cm $^{-2}$ were used in experiments that aimed at extending the sensitivity of iSCAT beyond small GNPs.[7] A thin sheet of mica, which can be locally atomically flat, was used as a substrate to reduce background variations by about 1 order of magnitude. Furthermore, a second photodiode was used as a reference for laser intensity fluctuations. In this manner, different kinds of single core−shell dots were successfully detected, even during dark photoblinking periods.[7]

Dye Molecules. iSCAT experiments on single quantum dots were soon followed by direct modulation-free detection of single dye molecules in extinction.[8,26] Here, an even better suppression of laser and background noise was crucial for reaching detection sensitivity beyond 10^{-6}. To address the instrumental laser noise, balanced detectors were used.[8] To improve the background, molecules were immersed in index-matching oil and investigated in transmission. Measurements at different wavelengths paved the way for single-molecule absorption spectroscopy.[26]

We note that dye molecules, quantum dots, and metal nanoparticles all have spectral resonances. However, even a small finite-sized dielectric nanoparticle can yield a large interferometric signal because the magnitude of the polarizability α is strongly influenced by the particle volume V.

Viruses. Shortly after its debut, iSCAT was applied to the detection of viruses and virus-like particles in systems such as microfluidic channels,[13] dielectric substrates,[33,43] artificial lipid membranes (see Figure 2b)[22,33] and more recently in biological cells.[31] Furthermore, iSCAT was combined with fluorescence to track a virus and a quantum dot attached to its surface simultaneously. This made it possible to visualize the nanoscopic binding domains of a single virus on an artificial membrane and to follow its rocking and tumbling motion.[22] In another study, iSCAT was used to image the position and orientation of bacteriophages on a functionalized surface and to resolve the stimulated ejection of DNA to a shot noise-limited precision of 4200 base pairs[44] (Figure 2c). Indeed, iSCAT holds a particularly high promise for tracking single viruses, which typically range in dimension from about 20 nm to beyond 200 nm with high spatial resolution at high speed and for very long times in a fully label-free fashion in order to visualize their interactions with cells and cellular environment.[31]

Proteins. The iSCAT signal of proteins is in the order of 1000 times smaller than that of an average virus because typical proteins are only a few nanometers in size, ranging between a few to a several hundred kDa in molecular weight. Nevertheless, it turns out that the scattering cross-section of a protein can be comparable to the absorption cross-section of a dye molecule. Thus, considering our earlier demonstration of single-molecule absorption, unlabeled single proteins should also be detectable by iSCAT.

The first results on iSCAT detection of single proteins were reported in early 2014 for myosin 5a with molecular weight of 500 kDa[34] and a series of smaller proteins down to BSA at 65 kDa,[21] (see Figure 2a,iv). A careful analysis of the contrast for proteins of different size, together with single-molecule fluorescence benchmarking and studies of binding kinetics, was used to demonstrate the exquisite sensitivity of iSCAT for label-free registration of single proteins with mass sensitivity.[21] This technique is superior to other biosensing solutions in many aspects. First, it enables one to count single proteins, bringing sensing to its ultimate limit. Second, detection occurs over a large continuous surface area. This is in contrast to several modern methods relying on plasmonic antennas[45] or optical microcavities.[46] Third, the fact that each protein arrival is localized in space and time provides invaluable information

DOI: 10.1021/acs.nanolett.9b01822
Nano Lett. 2019, 19, 4827−4835

about the interaction of the protein with the substrate (see Figure 3a), and finally, the experimental setup can be very

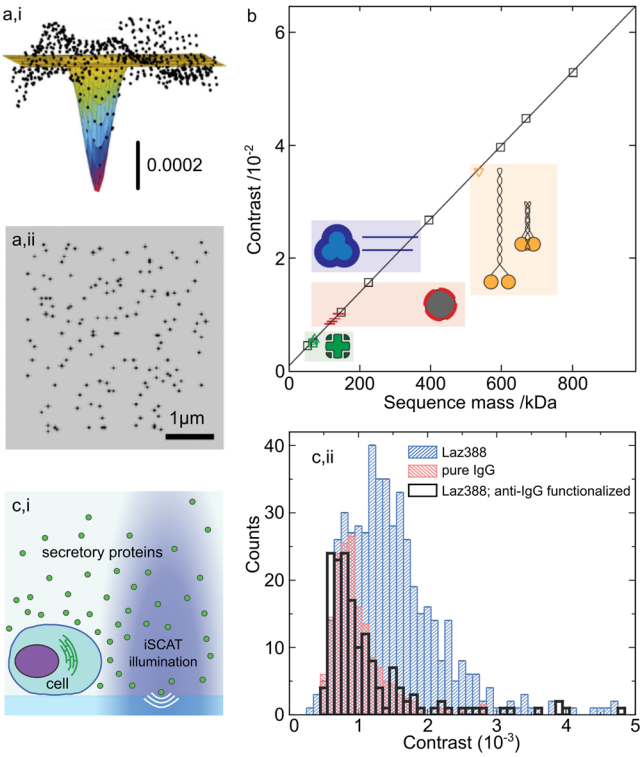

Figure 3. Sensitive detection of single proteins. (a,i) Nanometer localization of the PSF from a single protein. (a,ii) The super-resolved binding sites for many detected albumins across an imaging sequence. Adapted from ref 21. (b) Linear relation between the iSCAT signal and protein mass enables precise molecular weight calibration for different proteins and their complexes. Adapted from ref 25. (c,i) Illustration of the experimental arrangement for detecting the secretome from a single Laz388 cell. (c,ii) Histogram of contrast (mass) of secreted proteins, wherein the Immunoglobulin G (IgG) fraction can be identified. Adapted from ref 48.

compact and simple. However, as is the case in the great majority of biosensing platforms, including those relying on surface plasmons, microcavities, or mechanical oscillators, specificity has to be achieved via surface functionalization.[21]

The linearity of iSCAT contrast with particle volume also makes it sensitive to mass if one makes the reasonable assumption that the density of biological particles such as proteins does not vary much. This key property has been recently employed to demonstrate the applicability of iSCAT to quantitative mass spectrometry[25] (see Figure 3b). Furthermore, iSCAT was used to monitor the dynamics of molecular events such as protein aggregation, oligomerization, and cross-linking. Moreover, iSCAT has also been applied to a range of other protein studies such as mobility of single myosin-5 motor proteins on actin,[34] assembly of single tubulin dimers to a growing microtubule,[47] and motion of small proteins upon landing on a surface.[18] Other recent promising application of label-free single-protein detection include real-time investigation of cellular secretion[27,48] (see Figure 3c). This scheme has also been extended to an arrangement where surface plasmons in a thin gold surface replace freely traveling photons.[49]

Lipid Membranes. The early iSCAT studies of viruses on supported lipid bilayers[22,33] were followed by measurements on GNPs serving as a scattering label to investigate lipid diffusion. Here, GNPs are tethered to guest lipids mixed at low concentration within a synthetic lipid bilayer formed on glass substrates[18,23] (see, for example, Figure 4a). Particles as small

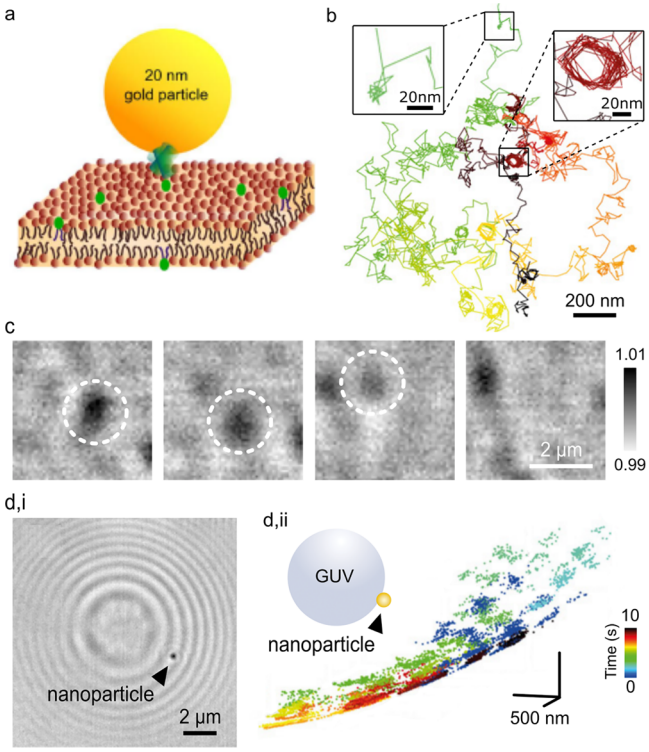

Figure 4. iSCAT study of lipid bilayers. (a) Schematic of a single GNP labeling lipids via a linker in a lipid bilayer membrane. Adapted from ref 40. (b) Diffusive trajectory of a membrane lipid over 5 s recorded at 1000 fps, revealing examples of confinement into nanoscale geometries (insets). Adapted from ref 18. (c) Image sequence of a transient liquid-ordered nanodomain (marked with a dashed circle) disappearing into the surrounding lipid bilayer membrane, taken from ref 51. (d,i) Newton rings appear in a wide-field iSCAT image of a GUV. A single Tat-coated polymer nanoparticle (marked by arrow) is bound to the outer surface. (d,ii) Schematic of a nanoparticle attached to a GUV, and a three-dimensional diffusional trajectory of the Tat-coated polymer nanoparticle, showing Brownian diffusion on a spherical surface. Color coding indicates temporal progression. Adapted from ref 18.

as 20 nm can be localized with nanometer precision at a speed of several thousand to one million frames per second,[17,18] allowing one to resolve transient nanoscale confinements (see, for example, Figure 4b). Here, it is important to bear in mind that achieving a high localization precision through long integration times, for example, as is done in fluorescence microscopy, would smear positional information and would, thus, mask fast dynamics.

In addition, iSCAT tracking of GNPs has been employed for discriminating between the varying mobilities of lipids diffusing in differently ordered phases of a bilayer membrane.[40] Here, we emphasize that it is challenging to carry out quantitative comparative studies of different measurement methods because each labeling strategy might introduce a systematic bias, leading to variations in the diffusion coefficients obtained.[41]

DOI: 10.1021/acs.nanolett.9b01822
Nano Lett. 2019, 19, 4827−4835

The high sensitivity of iSCAT can also be used to image small lipid entities directly without the need for a label, for example, small unilamellar vesicles (SUVs).[29] Moreover, docking and rupture of such SUVs with a size down to 20 nm were observed in real-time,[18,50] and transient dynamic phases within a supported membrane were examined[51] (see Figure 4c).

To avoid the influence of supporting substrates on the diffusion of lipids, free-standing model membranes have been studied with iSCAT. For example, a continuous lipid membrane can be spanned on an ultrathin substrate containing an array of micrometer-sized pores,[39] producing both supported and free-standing membranes. High-resolution iSCAT trajectories of GNP-tagged lipids confirmed that nanoscopic transient confinement events were only observed on the supported part of the substrate. An important asset of iSCAT tracking in this study was the ability to visualize diffusion in lipid bilayers prepared on gold-coated parts of the substrate, where fluorescence tracking is hampered by strong quenching.

Another promising option for investigating free membranes is to work with giant unilamellar vesicles (GUVs). Tracking on such a three-dimensional object is more challenging, but preliminary results have been obtained on the diffusion of viral-mimetic particles on GUVs with diameters in the range of tens of micrometers. Using iSCAT tracking, nanoparticles could be localized to nanometer precision in all dimensions over an extended range[18] (see Figure 4d).

Imaging Cells and Associated Elements. The past decade has witnessed a revival of interferometric imaging for cell biology applications. Previous efforts in holography and quantitative phase imaging, which have visualized larger cellular features,[52] are now being extended to the nanoscopic structures of the cell and its membrane. Some of the examples of the recent activities include profiling topology and membrane adhesion sites in wide-field[53,54] and confocal-scanning[55] configurations as well as growth, attachment, and retraction of bacterial pili.[56] Similarly, interferometric imaging can report on the nanomechanics of biomembranes,[57] including subnanometer twitching in the neuronal cell following execution of an action potential.[58]

A particularly challenging task in cell biology is to visualize diffusion and transport of viruses, proteins and other bioparticles on the cell surface. To date, however, transient cellular nanoscale effects have precluded satisfactory or compelling investigation by fluorescence methodologies because of limited measurement speed and duration. While the characteristic features of iSCAT microscopy make it highly suited to address these issues, the presence of large speckle-like background generated by the cell membrane and its corpus poses a daunting challenge. Nevertheless, recent efforts have shown that proper data analysis allows one to decipher the iSCAT signal of interest and trace three-dimensional trajectories of proteins and viruses[20,31,42] (see Figure 5). In particular, 3D iSCAT tracking of a transmembrane protein on a live cell has unraveled unprecedented details about heterogeneous mobility, nanoscopic confinement in clathrin-like lattice structures and directed diffusion along filopodia over long times[20] (see Figure 5b–d).

Discussion and Outlook. Interferometric signals have been at the heart of many imaging techniques, including conventional bright-field microscopy. However, the recent application of these methods to detection, imaging, and tracking of nano-objects as small as single proteins and molecules has opened a new chapter in microscopy under the heading of iSCAT, which emphasizes the importance of scattering as the central interaction mechanism. This Mini Review has discussed the rapid development of iSCAT over the past 15 years and has shown that its success relies on the fundamental property that the optical cross-section of even the smallest nanoparticle is fairly large to detect.

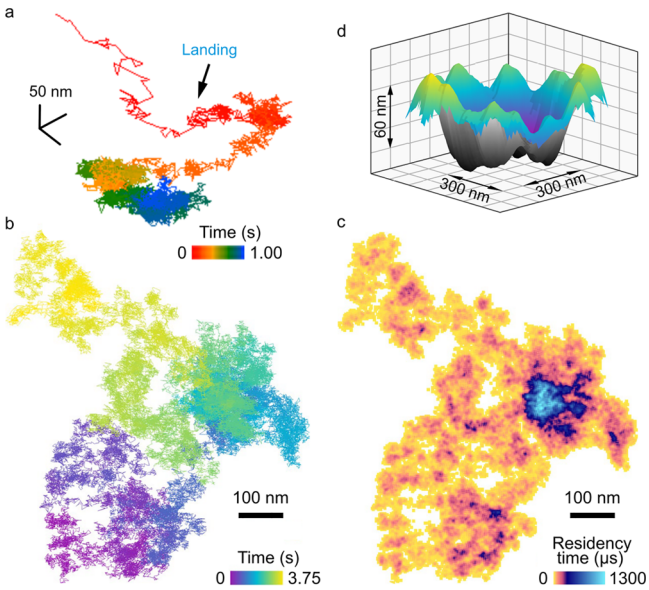

Figure 5. iSCAT tracking on the live cell. (a) Three-dimensional trajectory of a vaccinia virus interacting with a live HeLa cell surface. The virus is seen to undergo immediate nanoscale confinement. Trajectory recorded at 5000 fps. Adapted from ref 31. (b) A long trajectory of 75 000 data points recorded from a GNP-labeled transmembrane protein on a live HeLa cell, tracked to few-nanometer precision. (c) Temporal accumulated residency of the protein confirms regions of prolonged confinement. (d) Three-dimensional interpolated surface of a trajectory showing nanoscale confinement of the protein upon the membrane surface, consistent with confinement into a clathrin pit preceding endocytosis. (b–d) Adapted from ref 20.

The current state of the art in iSCAT achieves sensing of unlabeled bioparticles as small as about 50 kDa on well-defined surfaces such as functionalized cover glass within about hundred milliseconds.[21,25] On a live cell membrane, gold nanoparticles as small as 20 nm have been tracked in 3D at 50 μs temporal and about 5 nm spatial resolution.[20] It is important to emphasize that as it is not possible to quantify the limits of fluorescence microscopy in a general manner (for example, speed and sensitivity depend on the choice of fluorophore), it is similarly not possible to express the capabilities of iSCAT in a simple tabulated form either. The limit on the sensitivity and performance of iSCAT in imaging and tracking individual nanoparticles is imposed by the signal-to-noise ratio, which is in turn determined by parameters such as the scattering cross-section of the nanoparticle, illumination intensity, and choice of detector. The chief menacing factor for iSCAT imaging is background dynamics, which is specific to the specimen under study: the high sensitivity of iSCAT to nanoscopic amount of matter means that slightest variations in the optical path become imprinted onto the background.

Progress in detector technologies, data analysis, image processing, and machine learning promise to push the limits of iSCAT further. In particular, long-term 3D tracking of

DOI: 10.1021/acs.nanolett.9b01822
Nano Lett. 2019, 19, 4827–4835

nanoparticles such as viruses in more complex cellular environments and thin tissue would be of great advantage for fundamental medical research. Some of the challenges in achieving these goals as well as possible solutions are common to methods such as holography, quantitative phase imaging or imaging in scattering media. To this end, approaches such as two-color microscopy and wavefront engineering hold interesting promise for pushing the limits of iSCAT microscopy. Thus, it remains to be seen to what extent iSCAT might contribute to label-free imaging of cellular structures as a whole, that is, beyond tracking isolated nanoparticles.

From a technological point of view, the simplicity of the architecture of an iSCAT microscope makes it ideally suited to miniaturization into a compact instrument or integration into commercial microscope stations. One can, therefore, expect iSCAT to have a widespread impact in nanobiology, diagnostics, laboratory analytics, and materials research.

AUTHOR INFORMATION

Corresponding Author

*E-mail: vahid.sandoghdar@mpl.mpg.de.

ORCID

Richard W. Taylor: 0000-0002-0028-0677

Notes

The authors declare no competing financial interest.

ACKNOWLEDGMENTS

We are grateful to many fantastic group members, former (T. Kalkbrenner, K. Lindfors, P. Stoller, V. Jacobsen, E. Klotzsch, H. Ewers, P. Kukura, M. Celebrano, M. Piliarik, C.-L. Hsieh, J. Ehrig, S. Spindler, and M. McDonald) and present (M. Dahmardeh, H. Mirzaalian Dastjerdi, A. Gemeinhardt, M. Kaller, A. Kashkanova, K. König, M. Küppers, R. Gholami Mahmoodabadi, M. Mazaheri, F. Nicoli, and Y. Tuna), who are responsible for the success of iSCAT in our laboratories. We also thank the Alexander von Humboldt Foundation for their generous support in the context of a Humboldt Professorship (V.S.) and Postdoctoral Fellowship (R.W.T.) as well the Max Planck Society for continuous support.

REFERENCES

(1) Taylor, R. W.; Sandoghdar, V. Interferometric Scattering (iSCAT) Microscopy & Related Techniques. In *Label-Free Super-Resolution Microscopy*; Astratov, V., Ed.; Springer, 2019; ISBN 978-3-030-21722-8.

(2) Bohren, C. F.; Huffman, D. R. *Absorption and Scattering of Light by Small Particles*; John Wiley & Sons, Inc., 1983.

(3) Zumofen, G.; Mojarad, N. M.; Sandoghdar, V.; Agio, M. Perfect Reflection of Light by an Oscillating Dipole. *Phys. Rev. Lett.* **2008**, *101*, 180404.

(4) Mojarad, N. M.; Sandoghdar, V.; Agio, M. Plasmon spectra of nanospheres under a tightly focused beam. *J. Opt. Soc. Am. B* **2008**, *25*, 651−658.

(5) Loudon, R. *The Quantum Theory of Light*; Oxford University Press: Oxford, U.K., 2000.

(6) Wrigge, G.; Hwang, J.; Gerhardt, I.; Zumofen, G.; Sandoghdar, V. Exploring the limits of single emitter detection in fluorescence and extinction. *Opt. Express* **2008**, *16*, 17358−17365.

(7) Kukura, P.; Celebrano, M.; Renn, A.; Sandoghdar, V. Imaging a Single Quantum Dot When It Is Dark. *Nano Lett.* **2009**, *9*, 926−929.

(8) Kukura, P.; Celebrano, M.; Renn, A.; Sandoghdar, V. Single-Molecule Sensitivity in Optical Absorption at Room Temperature. *J. Phys. Chem. Lett.* **2010**, *1*, 3323−3327.

(9) Plakhotnik, T.; Palm, V. Interferometric Signatures of Single Molecules. *Phys. Rev. Lett.* **2001**, *87*, 183602.

(10) Boyer, D.; Tamarat, P.; Maali, A.; Lounis, B.; Orrit, M. Photothermal Imaging of Nanometer-Sized Metal Particles Among Scatterers. *Science* **2002**, *297*, 1160−1163.

(11) Lindfors, K.; Kalkbrenner, T.; Stoller, P.; Sandoghdar, V. Detection and Spectroscopy of Gold Nanoparticles Using Supercontinuum White Light Confocal Microscopy. *Phys. Rev. Lett.* **2004**, *93*, No. 037401.

(12) Arbouet, A.; Christofilos, D.; Del Fatti, N.; Vallée, F.; Huntzinger, J. R.; Arnaud, L.; Billaud, P.; Broyer, M. Direct Measurement of the Single-Metal-Cluster Optical Absorption. *Phys. Rev. Lett.* **2004**, *93*, 127401.

(13) Ignatovich, F. V.; Novotny, L. Real-Time and Background-Free Detection of Nanoscale Particles. *Phys. Rev. Lett.* **2006**, *96*, No. 013901.

(14) Jacobsen, V.; Stoller, P.; Brunner, C.; Vogel, V.; Sandoghdar, V. Interferometric optical detection and tracking of very small gold nanoparticles at a water-glass interface. *Opt. Express* **2006**, *14*, 405−414.

(15) Liebel, M.; Hugall, J. T.; van Hulst, N. F. Ultrasensitive Label-Free Nanosensing and High-Speed Tracking of Single Proteins. *Nano Lett.* **2017**, *17*, 1277−1281.

(16) Cole, D.; Young, G.; Weigel, A.; Sebesta, A.; Kukura, P. Label-Free Single-Molecule Imaging with Numerical-Aperture-Shaped Interferometric Scattering Microscopy. *ACS Photonics* **2017**, *4*, 211−216.

(17) Lin, Y.-H.; Chang, W.-L.; Hsieh, C.-L. Shot-noise limited localization of single 20 nm gold particles with nanometer spatial precision within microseconds. *Opt. Express* **2014**, *22*, 9159−9170.

(18) Spindler, S.; Ehrig, J.; König, K.; Nowak, T.; Piliarik, M.; Stein, H. E.; Taylor, R. W.; Garanger, E.; Lecommandoux, S.; Alves, I. D.; Sandoghdar, V. Visualization of lipids and proteins at high spatial and temporal resolution via interferometric scattering (iSCAT) microscopy. *J. Phys. D: Appl. Phys.* **2016**, *49*, 274002.

(19) Wäldchen, S.; Lehmann, J.; Klein, T.; van de Linde, S.; Sauer, M. Light-induced cell damage in live-cell super-resolution microscopy. *Sci. Rep.* **2015**, *5*, 15348.

(20) Taylor, R. W.; Gholami Mahmoodabadi, R.; Rauschenberger, V.; Giessl, A.; Schambony, A.; Sandoghdar, V. Interferometric scattering microscopy reveals microsecond nanoscopic protein motion on a live cell membrane. *Nat. Photonics* **2019**, *13*, 480−487.

(21) Piliarik, M.; Sandoghdar, V. Direct optical sensing of single unlabelled proteins and super-resolution imaging of their binding sites. *Nat. Commun.* **2014**, *5*, 4495.

(22) Kukura, P.; Ewers, H.; Müller, C.; Renn, A.; Helenius, A.; Sandoghdar, V. Highspeed nanoscopic tracking of the position and orientation of a single virus. *Nat. Methods* **2009**, *6*, 923−927.

(23) Hsieh, C.-L.; Spindler, S.; Ehrig, J.; Sandoghdar, V. Tracking Single Particles on Supported Lipid Membranes: Multimobility Diffusion and Nanoscopic Confinement. *J. Phys. Chem. B* **2014**, *118*, 1545−1554.

(24) Cheng, C.-Y.; Hsieh, C.-L. Background Estimation and Correction for High-Precision Localization Microscopy. *ACS Photonics* **2017**, *4*, 1730−1739.

(25) Young, G.; Hundt, N.; Cole, D.; Fineberg, A.; Andrecka, J.; Tyler, A.; Olerinyova, A.; Ansari, A.; Marklund, E. G.; Collier, M. P.; Chandler, S. A.; Tkachenko, O.; Allen, J.; Crispin, M.; Billington, N.; Takagi, Y.; Sellers, J. R.; Eichmann, C.; Selenko, P.; Frey, L.; Riek, R.; Galpin, M. R.; Struwe, W. B.; Benesch, J. L. P.; Kukura, P. Quantitative mass imaging of single biological macromolecules. *Science* **2018**, *360*, 423−427.

(26) Celebrano, M.; Kukura, P.; Renn, A.; Sandoghdar, V. Single-molecule imaging by optical absorption. *Nat. Photonics* **2011**, *5*, 95−98.

(27) Gemeinhardt, A.; McDonald, M. P.; König, K.; Aigner, M.; Mackensen, A.; Sandoghdar, V. Label-Free Imaging of Single Proteins Secreted from Living Cells via iSCAT Microscopy. *J. Visualized Exp.* **2018**, *141*, No. e58486.

DOI: 10.1021/acs.nanolett.9b01822
Nano Lett. 2019, 19, 4827−4835

(28) Jacobsen, V.; Klotzsch, E.; Sandoghdar, V. Interferometric detection and tracking of nanoparticles. In *Nano Biophotonics: Science and Technology*; Masuhara, H., Kawata, S., Tokunaga, F., Eds.; Elsevier: Oxford, U.K., 2000; Vol. 3, Chapter 9.
(29) Krishnan, M.; Mojarad, N.; Kukura, P.; Sandoghdar, V. Geometry-induced electrostatic trapping of nanometric objects in a fluid. *Nature* **2010**, *467*, 692−695.
(30) Sevenler, D.; Avci, O.; Ünlü, M. S. Quantitative interferometric reflectance imaging for the detection and measurement of biological nanoparticles. *Biomed. Opt. Express* **2017**, *8*, 2976−2989.
(31) Huang, Y.-F.; Zhuo, G.-Y.; Chou, C.-Y.; Lin, C.-H.; Chang, W.; Hsieh, C.-L. Coherent Brightfield Microscopy Provides the Spatiotemporal Resolution To Study Early Stage Viral Infection in Live Cells. *ACS Nano* **2017**, *11*, 2575−2585.
(32) Trueb, J. T.; Avci, O.; Sevenler, D.; Connor, J. H.; Ünlü, M. S. Robust Visualization and Discrimination of Nanoparticles by Interferometric Imaging. *IEEE J. Sel. Top. Quantum Electron.* **2017**, *23*, 394.
(33) Ewers, H.; Jacobsen, V.; Klotzsch, E.; Smith, A. E.; Helenius, A.; Sandoghdar, V. Label-Free Optical Detection and Tracking of Single Virions Bound to Their Receptors in Supported Membrane Bilayers. *Nano Lett.* **2007**, *7*, 2263−2266.
(34) Ortega Arroyo, J.; Andrecka, J.; Spillane, J. M.; Billington, N.; Takagi, Y.; Sellers, J. R.; Kukura, P. Label-Free, All-Optical Detection, Imaging, and Tracking of a Single Protein. *Nano Lett.* **2014**, *14*, 2065−2070.
(35) Holanovà, K.; Vala, M.; Piliarik, M. Optical imaging and localization of prospective scattering labels smaller than a single protein. *Opt. Laser Technol.* **2019**, *109*, 323−327.
(36) Stoller, P.; Jacobsen, V.; Sandoghdar, V. Measurement of the complex dielectric constant of a single gold nanoparticle. *Opt. Lett.* **2006**, *31*, 2474−2476.
(37) Lee, I.-B.; Moon, H.-M.; Joo, J.-H.; Kim, K.-H.; Hong, S.-C.; Cho, M. Interferometric Scattering Microscopy with Polarization-Selective Dual Detection Scheme: Capturing the Orientational Information of Anisotropic Nanometric Objects. *ACS Photonics* **2018**, *5*, 797−804.
(38) Fringes, S.; Skaug, M.; Knoll, A. W. *In situ* contrast calibration to determine the height of individual diffusing nanoparticles in a tunable confinement. *J. Appl. Phys.* **2016**, *119*, No. 024303.
(39) Spindler, S.; Sibold, J.; Gholami Mahmoodabadi, R.; Steinem, C.; Sandoghdar, V. High-Speed Microscopy of Diffusion in Pore-Spanning Lipid Membranes. *Nano Lett.* **2018**, *18*, 5262−5271.
(40) Wu, H.-M.; Lin, Y.-H.; Yen, T.-C.; Hsieh, C.-L. Nanoscopic substructures of raft-mimetic liquid-ordered membrane domains revealed by highspeed single-particle tracking. *Sci. Rep.* **2016**, *6*, 20542.
(41) Reina, F.; Galiani, S.; Shrestha, D.; Sezgin, E.; de Wit, G.; Cole, D.; Lagerholm, B. C.; Kukura, P.; Eggeling, C. Complementary studies of lipid membrane dynamics using iSCAT and super-resolved fluorescence correlation spectroscopy. *J. Phys. D: Appl. Phys.* **2018**, *51*, 235401.
(42) de Wit, G.; Albrecht, D.; Ewers, H.; Kukura, P. Revealing Compartmentalized Diffusion in Living Cells with Interferometric Scattering Microscopy. *Biophys. J.* **2018**, *114*, 2945−2950.
(43) Daaboul, G. G.; Yurt, A.; Zhang, X.; Hwang, G. M.; Goldberg, B. B.; Ünlü, S. M. High-Throughput Detection and Sizing of Individual Low-Index Nanoparticles and Viruses for Pathogen Identification. *Nano Lett.* **2010**, *10*, 4727−4731.
(44) Goldfain, A. M.; Garmann, R. F.; Jin, Y.; Lahini, Y.; Manoharan, V. N. Dynamic Measurements of the Position, Orientation, and DNA Content of Individual Unlabeled Bacteriophages. *J. Phys. Chem. B* **2016**, *120*, 6130−6138.
(45) Zijlstra, P.; Paulo, P. M. R.; Orrit, M. Optical detection of single non-absorbing molecules using the surface plasmon resonance of a gold nanorod. *Nat. Nanotechnol.* **2012**, *7*, 379−382.
(46) Vollmer, F.; Arnold, S. Whispering gallery-mode biosensing: Label-free detection down to single molecules. *Nat. Methods* **2008**, *5*, 591−596.
(47) Mickolajczyk, K. J.; Geyer, E. A.; Kim, T.; Rice, L. M.; Hancock, W. O. Direct observation of individual tubulin dimers binding to growing microtubules. *Proc. Natl. Acad. Sci. U. S. A.* **2019**, *116*, 7314−7322.
(48) McDonald, M. P.; Gemeinhardt, A.; König, K.; Piliarik, M.; Schaffer, S.; Völkl, S.; Aigner, M.; Mackensen, A.; Sandoghdar, V. Visualizing Single-Cell Secretion Dynamics with Single-Protein Sensitivity. *Nano Lett.* **2018**, *18*, 513−519.
(49) Yang, Y.; Shen, G.; Wang, H.; Li, H.; Zhang, T.; Tao, N.; Ding, X.; Yu, H. Interferometric plasmonic imaging and detection of single exosomes. *Proc. Natl. Acad. Sci. U. S. A.* **2018**, *115*, 10275−10280.
(50) Andrecka, J.; Spillane, K. M.; Ortega-Arroyo, J.; Kukura, P. Direct Observation and Control of Supported Lipid Bilayer Formation with Interferometric Scattering Microscopy. *ACS Nano* **2013**, *7*, 10662−10670.
(51) de Wit, G.; Danial, J. S. H.; Kukura, P.; Wallace, M. I. Dynamic label-free imaging of lipid nanodomains. *Proc. Natl. Acad. Sci. U. S. A.* **2015**, *112*, 12299−12303.
(52) Choi, W.; Fang-Yen, C.; Badizadegan, K.; Oh, S.; Lue, N.; Dasari, R. R.; Feld, M. S. Tomographic phase microscopy. *Nat. Methods* **2007**, *4*, 717−719.
(53) Klein, K.; Maier, T.; Hirschfeld-Warneken, V. C.; Spatz, J. P. Marker-Free Phenotyping of Tumor Cells by Fractal Analysis of Reflection Interference Contrast Microscopy Images. *Nano Lett.* **2013**, *13*, 5474−5479.
(54) Park, J.-S.; Lee, I.-B.; Moon, H.-M.; Joo, J.-H.; Kim, K.-H.; Hong, S.-C.; Cho, M. Label-free and live cell imaging by interferometric scattering microscopy. *Chem. Sci.* **2018**, *9*, 2690−2697.
(55) Matsuzaki, T.; Sazaki, G.; Suganuma, M.; Watanabe, T.; Yamazaki, T.; Tanaka, M.; Nakabayashi, S.; Yoshikawa, H. Y. High Contrast Visualization of Cell−Hydrogel Contact by Advanced Interferometric Optical Microscopy. *J. Phys. Chem. Lett.* **2014**, *5*, 253−257.
(56) Talà, L.; Fineberg, A.; Kukura, P.; Persat, A. Pseudomonas aeruginosa orchestrates twitching motility by sequential control of type IV pili movements. *Nat. Microbiol.* **2019**, *4*, 774−780.
(57) Biswas, A.; Alex, A.; Sinha, B. Cell Membrane Fluctuations Reveals Their Active Regulation and Transient Heterogeneities. *Biophys. J.* **2017**, *113*, 1768−1781.
(58) Yang, Y.; Liu, X.-W.; Wang, H.; Yu, H.; Guan, Y.; Wang, S.; Tao, N. Imaging Action Potential in Single Mammalian Neurons by Tracking the Accompanying Sub-Nanometer Mechanical Motion. *ACS Nano* **2018**, *12*, 4186−4193.

DOI: 10.1021/acs.nanolett.9b01822
Nano Lett. 2019, 19, 4827−4835